AD-A044 215 NAVAL RESEARCH LAB WASHINGTON D C F/G 11/6
SEM OBSERVATIONS OF FRACTURE SURFACES OF FATIGUE SPECIMENS OF A--ETC(U)
AUG 77 F A SMIDT, V PROVENZANO

UNCLASSIFIED NRL-8133 NL

| OF |
AD
A044 215

END
DATE
FILMED
10-77
DDC

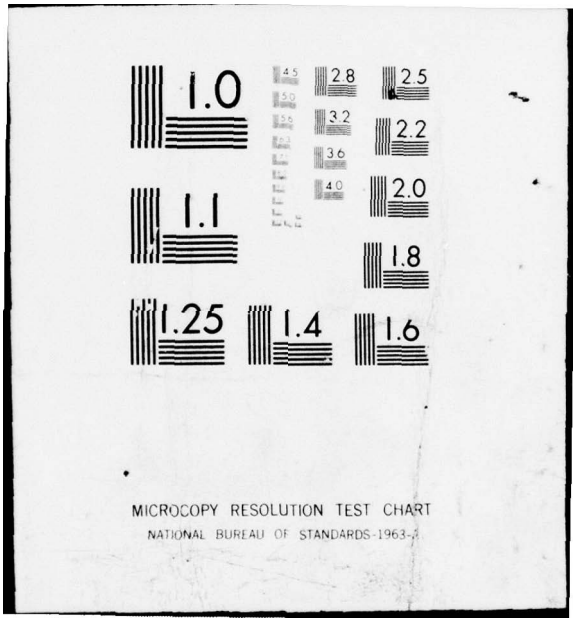
1.0
1.1
1.25
1.4
1.6
1.8
2.0
2.2
2.5
2.8
3.2
3.6
4.0
4.5
5.0
5.6
MICROCOPY RESOLUTION TEST CHART
NATIONAL BUREAU OF STANDARDS-1963-A

NRL Report 8133

SEM Observations of Fracture Surfaces of Fatigue Specimens of Annealed Type 316 Stainless Steel

F. A. SMIDT, JR., AND V. PROVENZANO

Thermostructural Materials Branch
Engineering Materials Division

August 10, 1977

NAVAL RESEARCH LABORATORY
Washington, D.C.

SECURITY CLASSIFICATION OF THIS PAGE (When Data Entered)

REPORT DOCUMENTATION PAGE

READ INSTRUCTIONS BEFORE COMPLETING FORM

1. REPORT NUMBER: NRL Report 8133	2. GOVT ACCESSION NO.
3. RECIPIENT'S CATALOG NUMBER	
4. TITLE (and Subtitle): SEM Observations of Fracture Surfaces of Fatigue Specimens of Annealed Type 316 Stainless Steel.	5. TYPE OF REPORT & PERIOD COVERED: Final report on a phase of a continuing NRL problem.
	6. PERFORMING ORG. REPORT NUMBER
7. AUTHOR(s): F. A. Smidt, Jr., and V. Provenzano	8. CONTRACT OR GRANT NUMBER(s)
9. PERFORMING ORGANIZATION NAME AND ADDRESS: Naval Research Laboratory, Washington, D. C. 20375	10. PROGRAM ELEMENT, PROJECT, TASK AREA & WORK UNIT NUMBERS: NRL Problem M01-14; RR 022-11
11. CONTROLLING OFFICE NAME AND ADDRESS: Department of the Navy, Office of Naval Research, Arlington, Va. 22217	12. REPORT DATE: August 10, 1977
	13. NUMBER OF PAGES: 27
14. MONITORING AGENCY NAME & ADDRESS(if different from Controlling Office)	15. SECURITY CLASS. (of this report): Unclassified
	15a. DECLASSIFICATION/DOWNGRADING SCHEDULE

16. DISTRIBUTION STATEMENT (of this Report)

Approved for public release; distribution unlimited.

DDC RECEIVED SEP 19 1977 B

17. DISTRIBUTION STATEMENT (of the abstract entered in Block 20, if different from Report)

18. SUPPLEMENTARY NOTES

19. KEY WORDS (Continue on reverse side if necessary and identify by block number)

20. ABSTRACT (Continue on reverse side if necessary and identify by block number)

The fracture surfaces of fatigue specimens of Type 316 stainless steel previously tested at elevated temperatures in air have been examined by scanning electron microscopy (SEM) to characterize the failure processes and to establish correlations with the previous studies of fatigue crack propagation. The SEM observations show three significantly different types of behavior which can be explained in terms of the differences in materials processing history and test conditions. Solution-annealed material tested at

(Continued) over

DD FORM 1 JAN 73 1473 EDITION OF 1 NOV 65 IS OBSOLETE S/N 0102-LF-014-6601

SECURITY CLASSIFICATION OF THIS PAGE (When Data Entered)

251950

20. Abstract (Continued)

800°F (427°C) exhibits a transgranular failure mode with fatigue striations indicative of a ductile failure process. Solution-annealed material tested at 1100°F (593°C) shows a change in failure mode to partially intergranular failure and an increase in crack propagation rate relative to the tests at 800°F (427°C). Imposition of a hold time further increases the proportion of the surface characterized by intertranular failure, and the crack growth rate also increases. Material aged at 1100°F (593°C) and tested at 1100°F (593°C) shows a return to the transgranular failure mode and a lower crack growth rate than solution annealed material tested at 1100°F (593°C). The imposition of a hold time period had no significant effect on the failure mode. The observations are consistent with a model in which grain boundary embrittlement caused by diffusion of oxygen ahead of the crack tip produces intergranular failure and an acceleration of crack growth rate.

Grain-boundary diffusion of oxygen at 427°C (800°F) is too slow to produce the embrittlement observed at 593°C (1100°F) in the solution-annealed material. Aging the material strengthens the grain boundaries so that intergranular failure does not occur.

The observations and the model developed in the present investigation provide a rational basis for explaining differences in the crack propagation behavior in fatigue tests of austenitic stainless steels tested at elevated temperature in air.

CONTENTS

SCANNING ELECTRON MICROSCOPE OBSERVATIONS OF FRACTURE SURFACES OF FATIGUE SPECIMENS OF ANNEALED TYPE 316 STAINLESS STEEL

INTRODUCTION

The prediction of crack growth rates in flawed structures subjected to cyclical loading is currently under active investigation. The problem is particularly difficult in the elevated temperature regime, where creep processes may cause relaxation of the crack tip stresses and where environmental effects may influence the crack behavior. Shahinian and Michel and their co-workers at NRL [1-3] have extensively examined fatigue crack propagation in the austenitic stainless steels Type 304 and 316. Their purpose was to characterize the influence of test temperature (427°C and 593°C) (800 and 1100°F), material conditions (solution annealed, cold worked, aged at 593°C (1100°F), and neutron irradiated), and hold time (0.1 and 1.0 min) on the crack propagation rate in single-edge-notched cantilever beam specimens cycled under zero-to-tension loading in air.

The purpose of the present investigation was twofold. First, the fracture surfaces of annealed Type 316 stainless steel specimens tested in previous investigations [1-3], and generously provided by those authors, were examined by scanning electron microscopy (SEM) to characterize the failure mode. Second, the SEM data and the fatigue crack propagation data previously generated [1-3] were critically examined from the microstructural perspective with the objective of searching for unifying principles to correlate the data. Those previous studies contained interpretations of the results based upon the information available at the time of the investigation. Insofar as possible, however, the present analysis has been done independently of the previous interpretations, to avoid bias and to find out if similar conclusions are reached when the subject is approached from the microstructural perspective. In many cases the conclusions are similar, as would be expected, but the microstructural approach has provided several new insights into the mechanisms of fatigue crack propagation.

The plan of presentation is first to briefly review both the experimental procedures under which the crack propagation data were obtained and the SEM techniques used to examine the specimens. Next, the SEM observations are presented in the context of the fatigue history for each specimen. Some of the unifying principles that provide a framework for interpreting and evaluating the results are then discussed. The next section contains a discussion and interpretation of the results for each of the three material and test-temperature conditions that showed a unique response. These were the solution-annealed material tested at 427°C (800°F), the solution-annealed material tested at 593°C (1100°F), and the aged material tested at 593°C (1100°F). The conclusions reached in previous studies [1-3] are then discussed in light of the additional information generated in this study, and some unresolved issues are cited. Finally, the conclusions and implications are summarized.

Manuscript submitted May 18, 1977.

EXPERIMENTAL PROCEDURE

Complete details of the materials, specimen history, fatigue test procedures, and data analysis methods have been previously reported [1-3]. Only the pertinent variables and techniques required to provide background for the reader are summarized in this report.

Single-edge-notched cantilever beam specimens were cycled under zero-to-tension loading to a constant maximum load at a frequency of 0.17 Hz using a sawtooth waveform, as shown in Fig. 1a. The tests were conducted at 427°C (800°F) and 593°C (1100°F) in an air environment. The effect of static loading (hold time) was examined by holding the maximum load for 0.1 and 1.0 min before returning to zero load, as shown in Fig. 1b. The Type 316 stainless steel tested in these experiments had a composition, in weight percent, of 0.060 C, 1.72 Mn, 0.012 P, 0.007 S, 0.40 Si, 17.30 Cr, 13.30 Ni, 2.33 Mo, 0.65 Cu, 0.30 Co, 0.012 Al, 0.003 Ti, and 0.0005 B. Material conditions examined included material solution-annealed at 1090°C (2000°F) for 1 h and material additionally aged for 5000 h in air at 593°C (1100°F). The fatigue data were analyzed to yield crack propagation rate da/dN as a function of the stress intensity factor range ΔK.

The SEM specimens were machined to a size of approximately 20.0 mm × 9.0 mm × 2.5 mm from the failed fatigue specimens. The fracture surfaces of most of the specimens were oxidized to some extent, depending on the previous fatigue test conditions. An initial attempt to clean the specimen surfaces utilized ultrasonic cleaning in acetone and alcohol. Where the ultrasonic cleaning was not effective, an inhibited HCl solution composed of 100 mℓ 6N HCl with 0.2 g hexamethylene-tetramine was used to remove the oxide film [4]. This oxide removal method does not attack the metal surface, as documented in the studies of Brooks and Lundin [5] and confirmed by the present observations. The specimens tested at 593°C (1100°F) had a particularly heavy and tenacious oxide layer that required an additional step in oxide removal processes: stripping with cellulose acetate tape. This technique is similar to the one used in preparing replicas of fracture surfaces [6]. After cleaning, the specimen was mounted to the SEM sample-holder adaptor with a conductive cement and was dried overnight in a dessicator.

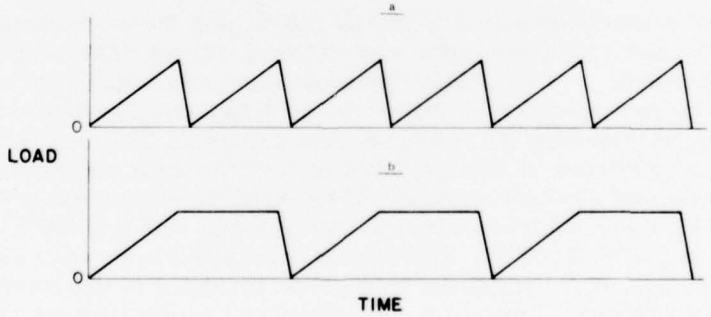

Fig. 1 — Waveforms used for fatigue testing [3]: (a) 0.17 Hz — zero hold time; (b) 0.1-and 1-min hold times

The specimens were examined on a Coates and Welter scanning electron microscope (SEM) using the secondary electron emission mode. At magnifications of 500X or less, the instrument was operated with the accelerating voltage in the Low Voltage Mode (840-900 V); at magnifications above 500X the High Voltage Mode (18-15.5 kV) was used. The specimen was positioned so that the fracture surface was oriented at an angle of 45° with respect to both the electron beam and the detector and so that the length of the specimen was parallel to a stage translation direction. This particular orientation lessens the amount of refocusing necessary when the specimen is laterally translated and also minimizes magnification corrections. Stereo pairs with a separation of 6° were taken of selected areas where required to distinguish topographic features.

EXPERIMENTAL RESULTS

Three distinguishable types of failure behavior were identified from the SEM examination of these AISI Type 316 stainless steel fatigue specimens. The failure modes appeared to be most strongly influenced by test temperature and thermomechanical history, but under certain conditions they were also influenced by hold time. The results are presented in the following sequence: (a) solution-annealed material tested at 427°C (800°F), for all hold times), (b) solution-annealed material tested at 593°C (1100°F) (for all hold times), and (c) material aged at 593°C (1100°F) for 5000 h and tested at 593°C (1100°F) (for all hold times). This sequence represents something of an ascending order in the complexity of the results.

The crack propagation data in the previous investigations [1-3] were analyzed and presented in the form of log da/dN vs log ΔK curves, which, for easy reference, are also included in this report. These curves were derived from graphical and computer analyses of the change in crack length during the fatigue test and from ΔK values corresponding to that crack length, which were calculated according to the expression for K in pure bending given by Gross and Srawley [7]. The results approximate a linear behavior when plotted as log da/dN vs log ΔK. Changes in slope of the curves are sometimes observed. Possible causes of these changes in slope are examined and their significance assessed in the section "Discussion of Test Results."

Consider first the solution-annealed material tested at 427°C (800°F). The crack growth rate data from the tests [3] is presented in Fig. 2. As can be seen in the figure, the growth rate per cycle increases from approximately 7.5×10^{-5} mm/cycle (3×10^{-6} in./cycle) at 22 MPa$\sqrt{\text{m}}$ (20 ksi$\sqrt{\text{in.}}$) to about 3.8×10^{-3} mm/cycle (1.5×10^{-4} in./cycle) at 55 MPa$\sqrt{\text{m}}$ (50 ksi$\sqrt{\text{in.}}$). In this range it approximates a linear behavior. At low magnifications the fracture surface shows a transgranular mode of failure with irregular topography from grain to grain. At high magnifications fatigue striations can be found on the surface, as illustrated in Fig. 3, for both low, 22 MPa$\sqrt{\text{m}}$ (20 ksi$\sqrt{\text{in.}}$), and high 44 MPa$\sqrt{\text{m}}$ (40 ksi$\sqrt{\text{in.}}$), ΔK regimes of the test. These striations are typical of those found in ductile metals [8] as a consequence of the alternate extension of the crack by shear and the subsequent compression of the crack tip region during the unloading part of the cycle. It is readily apparent that the striation spacings increase as one goes to higher ΔK values, and measurements of the striation spacing at both high and low ΔK show a close correlation with the calculated da/dN values. The imposition of a hold time had no noticable influence on either the crack growth rate, as can be seen in Fig. 2, or the appearance of the fracture surface, as can be seen in Fig. 4.

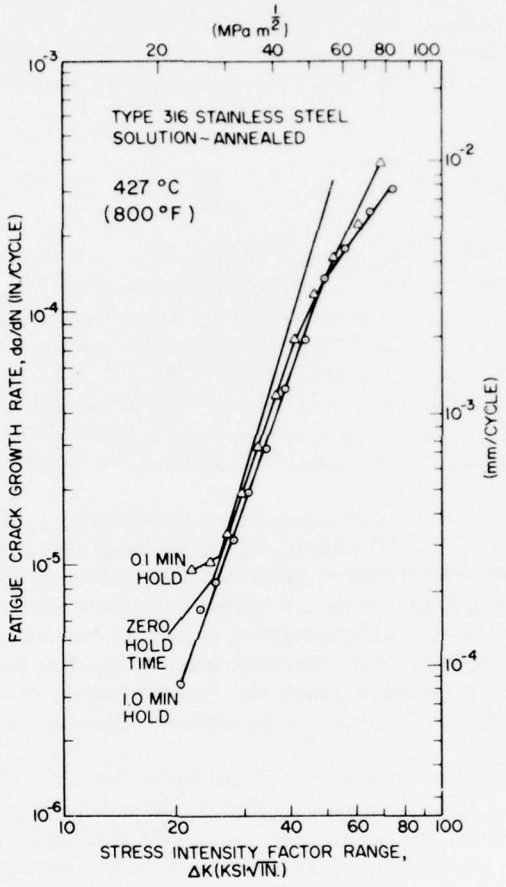

Fig. 2 — Effect of hold time on fatigue crack propagation rate da/dN in air at 427°C (800°F) for solution-annealed Type 316 stainless steel [3]

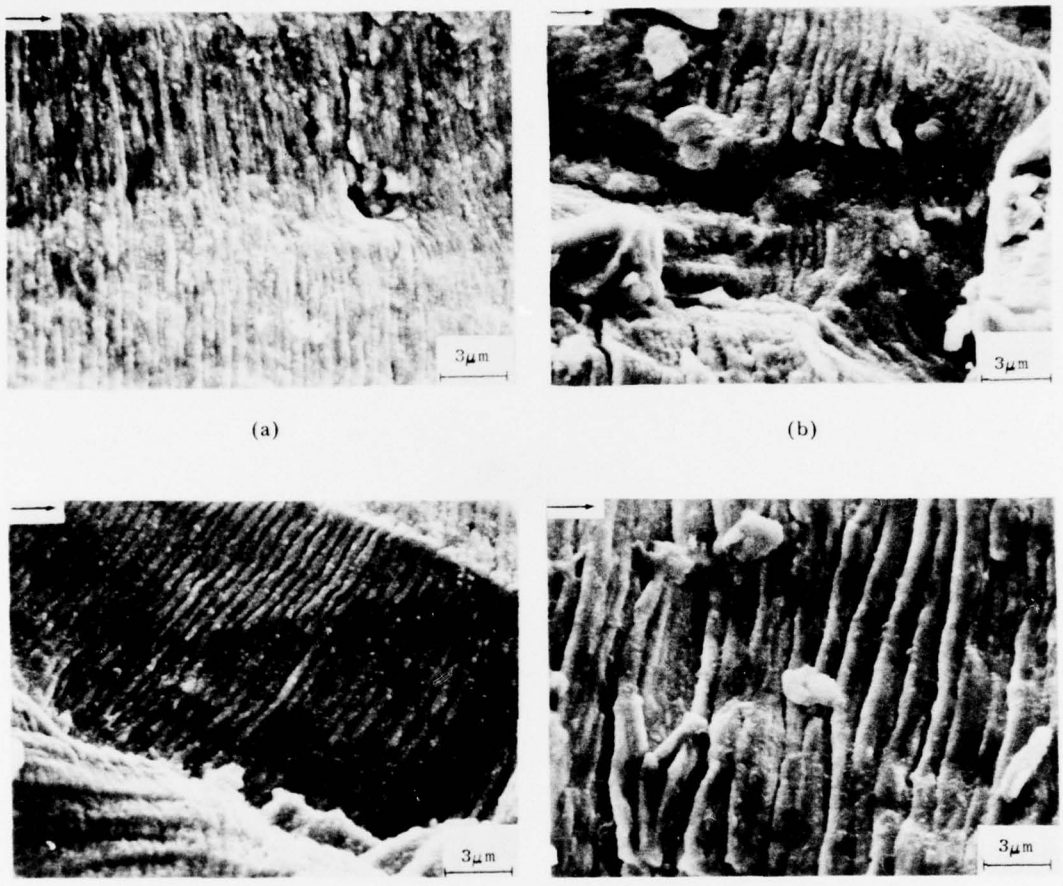

Fig. 3 — Fracture surfaces (SEM) of a solution-annealed stainless steel specimen tested at 427°C (800°F) with 0.1-min hold time. The SEM micrographs were taken at crack lengths that correspond to the following ΔK values: (a) 22 MPa$\sqrt{m}$ (20 ksi$\sqrt{in.}$), (b) 27.5 MPa$\sqrt{m}$ (25 ksi$\sqrt{in.}$), (c) 33 MPa$\sqrt{m}$ (30 ksi$\sqrt{in.}$), and (d) 44 MPa$\sqrt{m}$ (40 ksi$\sqrt{in.}$). Arrows indicate direction of macroscopic crack propagation. Transgranular features with distinct fatigue striations can be clearly seen in the micrographs.

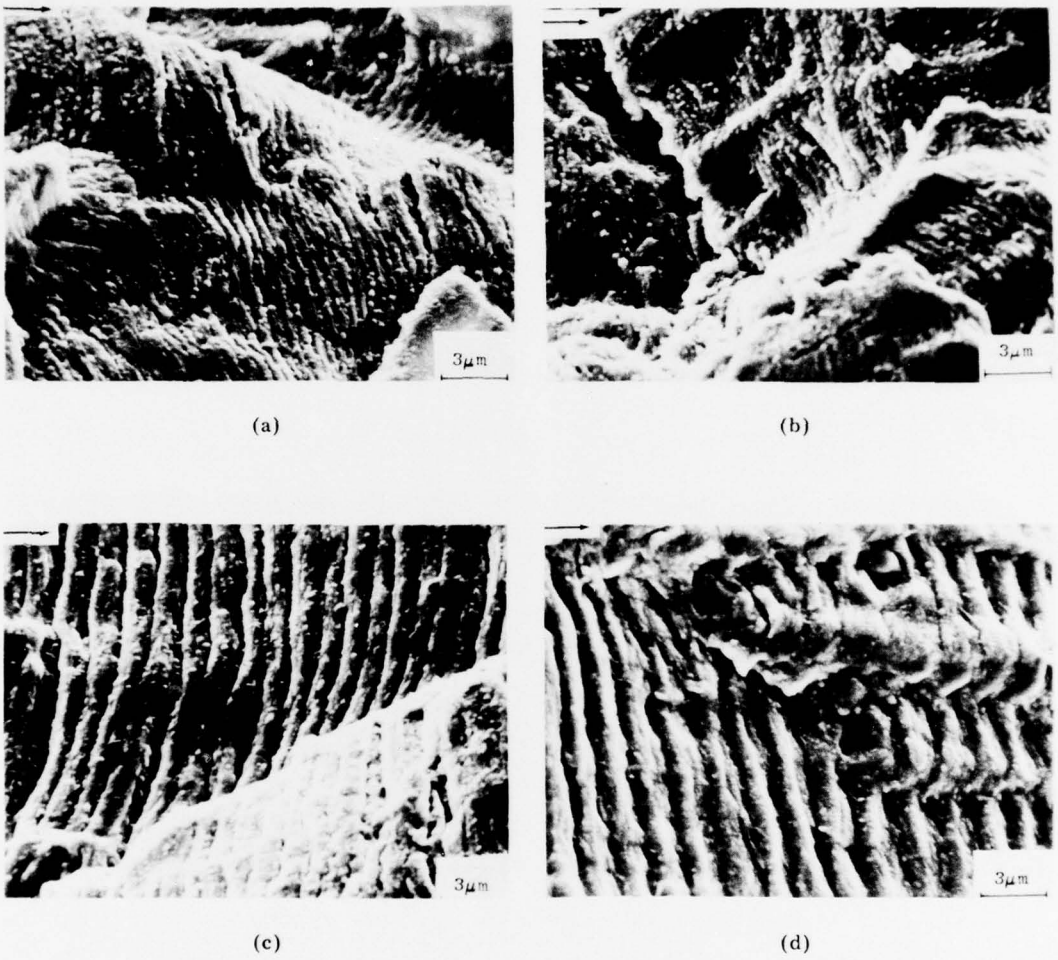

(a) (b)

(c) (d)

Fig. 4 — Fracture surfaces (SEM) of a solution-annealed stainless steel specimen tested at 427°C (800°F) with 1-min hold time. The SEM micrographs were taken at crack lengths that correspond to the following ΔK values: (a) 22 MPa$\sqrt{m}$ (20 ksi$\sqrt{in.}$), (b) 27.5 MPa$\sqrt{m}$ (25 ksi$\sqrt{in.}$), (c) 33 MPa$\sqrt{m}$ (30 ksi$\sqrt{in.}$), and (d) 44 MPa$\sqrt{m}$ (40 ksi$\sqrt{in.}$). Arrows show the direction of macroscopic crack propagation. As was the case for a hold time of 0.1 min, transgranular features with clear fatigue striations can be seen in the micrographs.

Crack growth rate data for the solution-annealed material tested at 593°C (1100°F) [3] is presented in Fig. 5. The crack growth rate for the specimen tested with no hold time increases from approximately 5×10^{-4} mm/cycle (2×10^{-5} in./cycle) at about 22 MPa$\sqrt{m}$ (20 ksi$\sqrt{in.}$) to about 3×10^{-3} mm/cycle (1.2×10^{-4} in./cycle) at about 55 MPa$\sqrt{m}$ (50 ksi$\sqrt{in.}$). This crack growth rate is higher than the growth rate at 427°C (800°F) for comparable values of ΔK. The crack growth rate curve is nearly linear in the ΔK range from 26 MPa$\sqrt{m}$ (24 ksi$\sqrt{in.}$) to about 44 MPa$\sqrt{m}$ (40 ksi$\sqrt{in.}$), but there are changes in slope both above and below the midrange region. The introduction of 0.1-and 1.0-min hold times during the fatigue cycle increases the crack growth rate da/dN, as compared to the test with no hold time. Above 44 MPa$\sqrt{m}$ (40 ksi$\sqrt{in.}$) the zero and 0.1-min hold time curves show an anomalous decrease in the slope. This is considered in more detail in the discussion of test results.

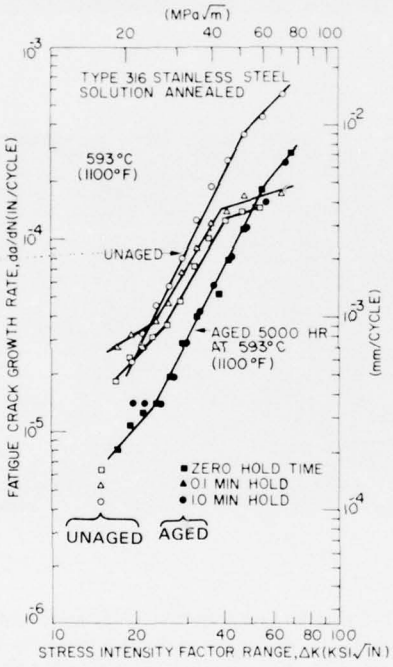

Fig. 5 — Effect of hold time on fatigue crack growth rate da/dN in air at 593° C (1100°F) for unaged and thermally aged Type 316 stainless steel [3]

Typical SEM micrographs of the solution-annealed specimens tested at 593°C (1100°F) with no hold time are shown in Fig. 6. As in previous figures, these micrographs include representatives from regions of both low and high values of ΔK. For crack lengths up to 16mm (0.65 in.), which corresponds to a ΔK value of 33 MPa$\sqrt{m}$ (30 ksi$\sqrt{in.}$), the failure mode was mixed, containing areas where intergranular failure, as well as the more predominant transgranular failure mode, was clearly evident. At ΔK values above 33 MPa$\sqrt{m}$ (30 ksi$\sqrt{in.}$), the failure mode was transgranular, and clear striations were observed, as shown in Fig. 6.

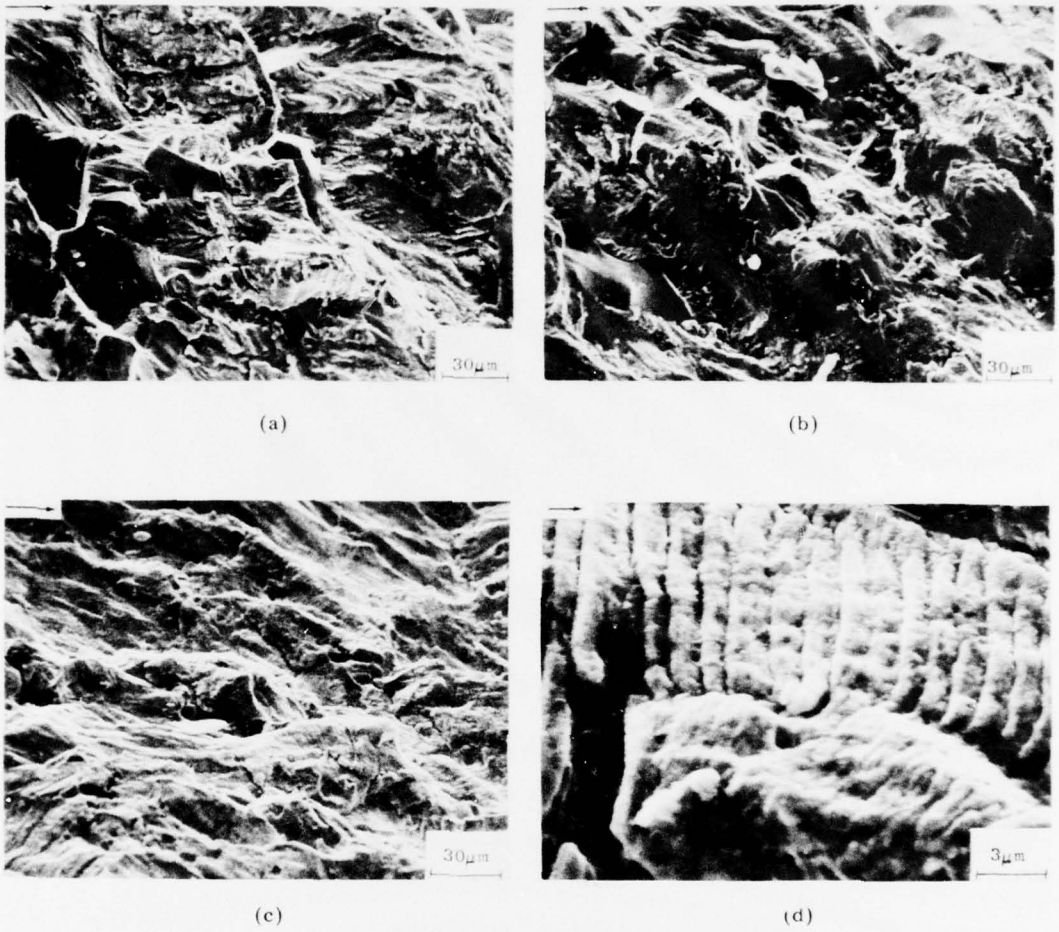

Fig. 6 — Fracture surfaces of a solution-annealed Type 316 stainless steel specimen tested at 593°C (1100°F) with zero hold time. The SEM micrographs were taken at crack lengths that correspond to the following ΔK values: (a) 22 MPa$\sqrt{m}$ (20 ksi$\sqrt{in.}$), (b) 27.5 MPa$\sqrt{m}$ (25 ksi$\sqrt{in.}$), (c) 33 MPa$\sqrt{m}$ (30 ksi$\sqrt{in.}$), and (d) 44 MPa$\sqrt{m}$ (40 ksi$\sqrt{in.}$). Arrows show direction of macroscopic crack propagation.

The striation spacings again correlate with the da/dN values calculated in the fatigue data analysis. The introduction of a 1-min hold time during the fatigue cycle caused the material to fail intergranularly for all values of ΔK. This is clearly evident in the SEM micrographs in Fig. 7. As mentioned earlier, there was some indication of a hold time effect at 593°C (1100°F) in the fatigue data, although the trend was not clearly outside the limits of experimental scatter. The SEM micrographs clearly show a change in microstructure and confirm the presence of a hold time effect.

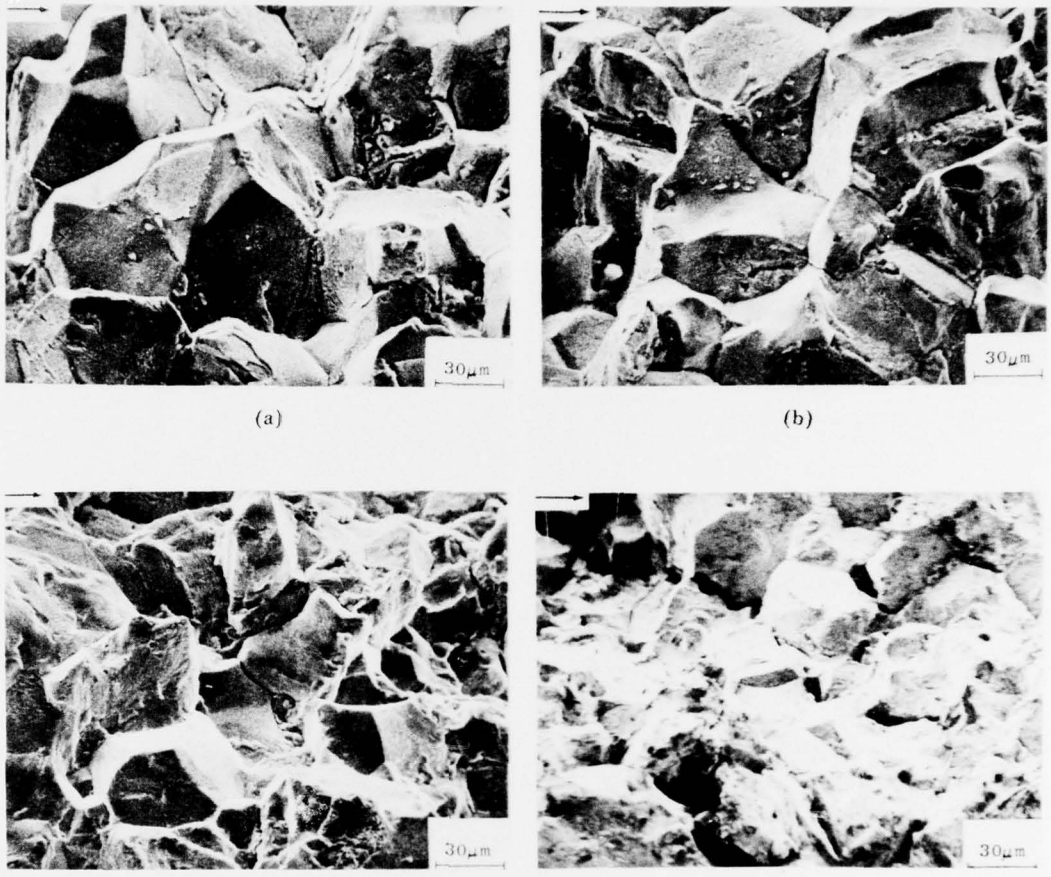

Fig. 7 — Fracture surfaces of a solution-annealed Type 316 stainless steel specimen tested at 593°C (1100°F) with 1-min hold time. The SEM micrographs were taken at crack lengths that correspond to the following ΔK values: (a) 22 MPa$\sqrt{\text{in.}}$), (b) 27.5 MPa$\sqrt{\text{m}}$ (25 ksi$\sqrt{\text{in.}}$), (c) 33 MPa$\sqrt{\text{m}}$ (30 ksi$\sqrt{\text{in.}}$), and (d) 44 MPa$\sqrt{\text{m}}$ (40 ksi$\sqrt{\text{in.}}$). Arrows show direction of macroscopic crack propagation. Micrographs show that the failure mode was mostly intergranular for all ΔK values.

Figure 5 also shows crack propagation data for the aged material tested at 593°C (1100°F) [3]. As can be seen in the figure, the growth per cycle goes from approximately 2×10^{-4} mm/cycle (8×10^{-5} in./cycle) at a ΔK value of about 22 MPa$\sqrt{\text{m}}$ (20 ksi$\sqrt{\text{in.}}$), to approximately 7.5×10^{-3} mm/cycle (3×10^{-4} in./cycle) at a ΔK value of about 72 MPa$\sqrt{\text{m}}$ (65 ksi $\sqrt{\text{in.}}$). Except for the slight variations in the slope at the lower and upper ends of the curve, the data are linear on the log-log plot. The crack growth rate in the aged material is less than that in the solution-annealed material at this same temperature but is slightly faster than the growth rate in the solution-annealed material tested at 427°C (800°F). The slope of the log da/dN vs log ΔK curve is about the same as that found in the solution-annealed specimens tested at the same temperature. No hold time effect is apparent in the fatigue data.

Typical SEM micrographs of the zero hold time specimens are shown in Fig. 8a and 8b of the 1-min hold time specimens in Fig. 8c and 8d. The failure mode is transgranular but of a different nature than that observed for the test and material conditions previously described. The fracture surface shows features of microvoid coalescense, which is typical of a ductile rupture failure process. Inclusions, probably the carbide precipitates formed during aging, can be clearly seen in all panels of Fig. 8 as the light-colored features in the center of the microvoids. The microvoids appear to be larger in the specimen tested with 1-min hold time.

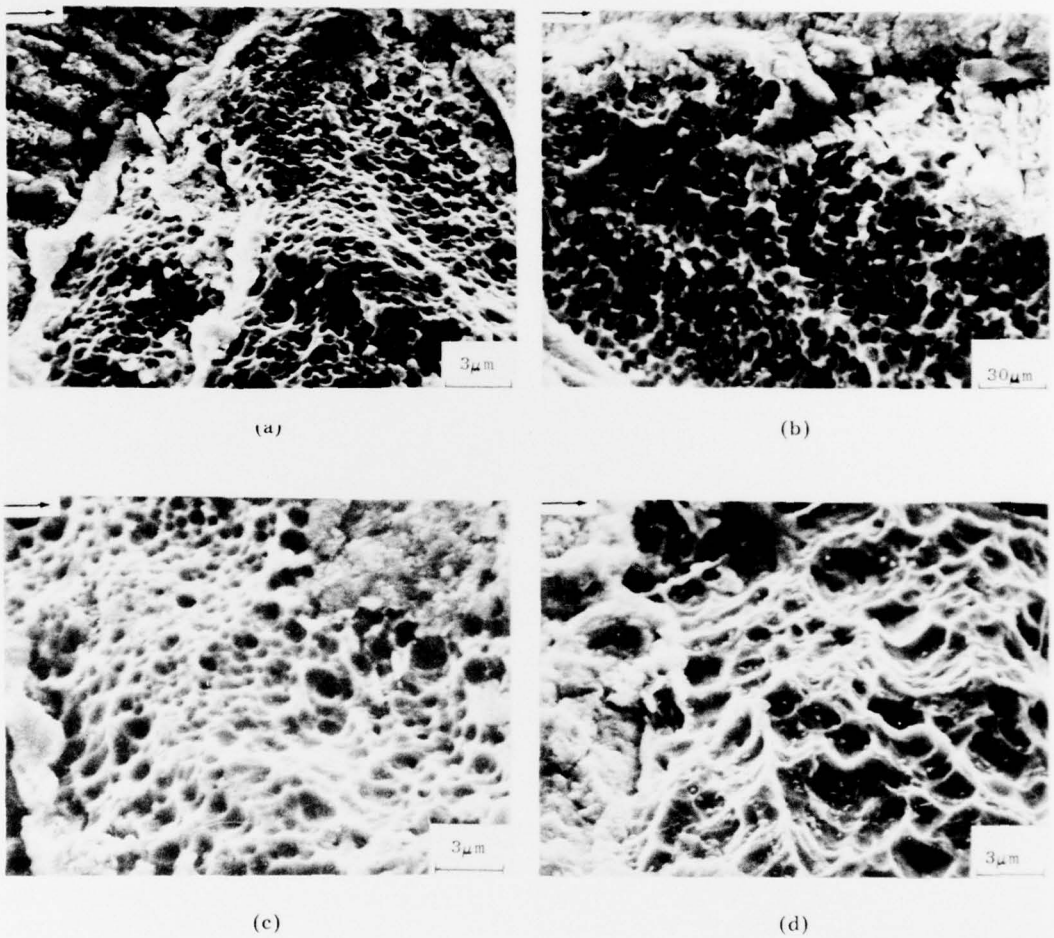

(a) (b)

(c) (d)

Fig. 8 — Fracture surfaces (SEM) of solution-annealed, thermally aged Type 316 stainless steel specimens tested at 593°C (1100°F). Specimens (a) and (b) were tested with zero hold time; (c) and (d) were tested with 1-min hold time. The SEM micrographs were taken at crack lengths that correspond to the following ΔK values: (a) 22 MPa$\sqrt{m}$ (20 ksi$\sqrt{in.}$), (b) 27.5 MPa$\sqrt{m}$ (25 ksi$\sqrt{in.}$), (c) 22 MPa$\sqrt{m}$ (20 ksi$\sqrt{in.}$), and (d) 27.5 MPa$\sqrt{m}$ (25 ksi$\sqrt{in.}$). Arrows show direction of macroscopic crack propagation. For both sets of test conditions the micrographs show that specimens failed transgranularly by microvoid coalesence. In the case of 1-min hold time, the void size tends to increase with higher ΔK value.

The voids also tend to increase in size with increasing ΔK. The basic fatigue features are the same in both specimens. That is, wherever the oxide layer has been removed by the cleaning process, microvoids can be seen (Fig. 8a-8d, 9a and 9c). In contrast, where the oxide layer still covers the fracture surface, striations are visible, especially in the later stages of crack growth when the ΔK values are high (Fig. 9b and d). The striation spacings compare quite well with the corresponding crack growth rates in the mechanical data.

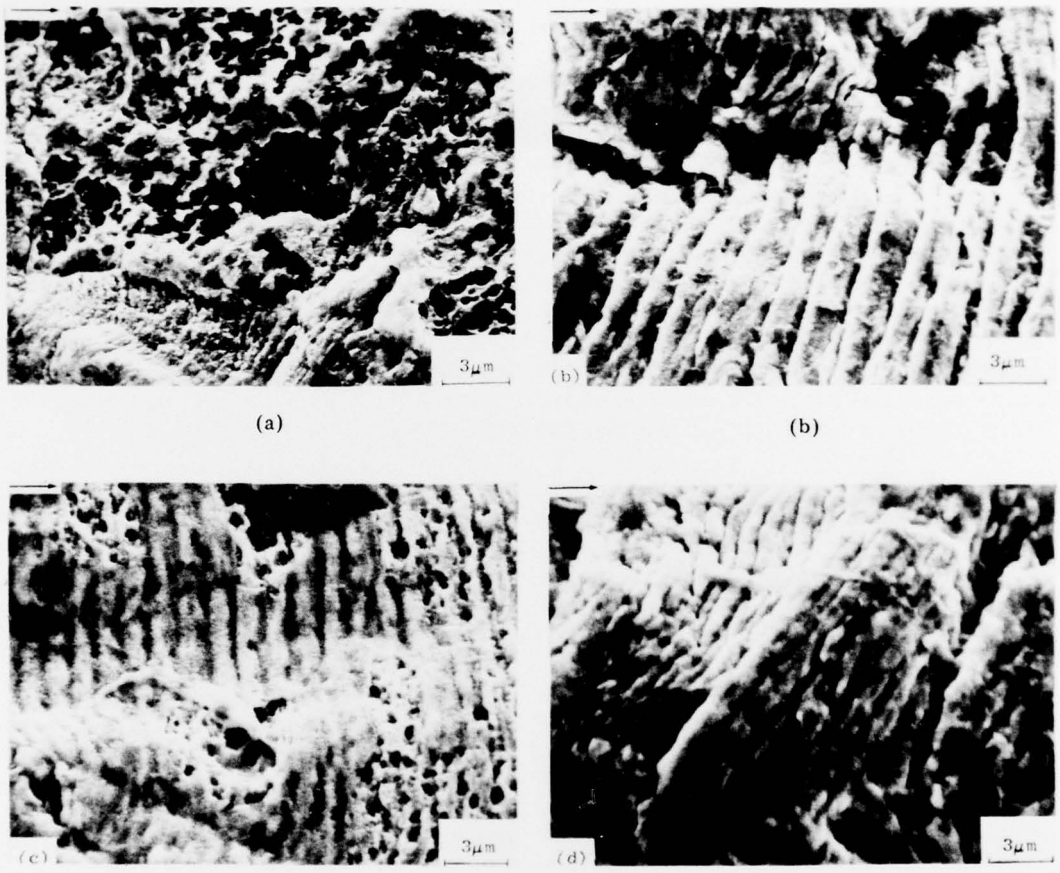

Fig. 9 — SEM micrographs of a solution-annealed thermally aged Type 316 stainless steel specimen tested at 593°C (1100°F). Specimens (a) and (b) were tested with no bold time; (c) and (d) were tested with bold time. The micrographs were taken at crack lengths corresponding to the following ΔK values: (a) 37.5 MPa$\sqrt{m}$ (35 ksi$\sqrt{in.}$), (b) 44 MPa$\sqrt{m}$ (40 ksi$\sqrt{in.}$), (c) 37.5 MPa$\sqrt{m}$ (35 ksi$\sqrt{in.}$), and (d) 44 MPa$\sqrt{m}$ (40 ksi$\sqrt{in.}$). Arrows show direction of macroscopic crack propagation. Microvoids can be seen wherever the oxide layer has been removed. Clear striations are visible where the oxide layer still covers the fracture surface.

DISCUSSION: A SEARCH FOR UNIFYING PRINCIPLES

The previous results show a variety of behaviors depending on the test conditions and thermomechanical history of the material. The cause-and-effect relationship of these various behaviors is not readily apparent. One of the primary objectives of this report is to attempt to identify behavioral trends in the data. A brief digression is therefore in order to review some of the unifying principles which have been found for fatigue in other materials and to suggest an approach based on deformation mechanism maps that makes maximum use of the microstructural information gained from the SEM observations. This discussion provides the framework for the interpretation and generalization of results to be discussed in detail in the following section. Those readers intimately familiar with the field may wish to scan this section, simply noting the rationale developed to support the conclusions in the later section.

An excellent review of behavioral trends in fatigue crack propagation (FCP) has been prepared by Spiedel [9]. His work provides the basis for suggesting several similar trends in the present work. The development of linear elastic fracture mechanics (LEFM) has provided the framework to define the test conditions under which fracture behavior is independent of specimen geometry. LEFM can also be applied to fatigue crack propagation to define geometry that will yield valid test results. Paris and Erdogan [10] found that a good correlation could be made of crack growth rate per cycle da/dN with the stress intensity factor K using an empirical relation of the form $da/dN = C(\Delta K)^n$ where ΔK is the range of K values and C and n are material parameters. A wide variety of materials shows linear behavior when the fatigue crack propagation data for purely elastic loading are displayed on log-log plots. As noted in the previous section, this analytical method was applied to the NRL results [1-3].

Speidel has shown that a further generalization can be made if one plots the data as a function of $\Delta K/E$, where E is the elastic modulus [9]. When this is done for tests *conducted in vacuum*, the crack propagation data for materials ranging from copper to molybdenum can be fitted to the same curve with a value for the exponent n of about 3.5. It further appears that tests conducted over a range of temperatures can be correlated by taking into account the temperature dependence of E, again with the provisos that the tests are in vacuum [11] and that loading is in the elastic range. These observations provide a basis for searching for behavioral trends.

Further generalizations about FCP data can be made if one considers the limits of ΔK to be expected. An upper limit on ΔK will obviously be imposed by the fracture toughness of the material, and the approach to this limit would be manifested as a rapid increase in the slope of the crack growth rate curve. Plastic overload would also terminate the test when instability and necking occurred. Intervention of both of these phenomena would cause an *increase* in slope as the limit was approached. A lower limit or threshold ΔK, below which the crack will not propagate, also has been postulated but is not firmly established. No effects arising from LEFM would produce a change in slope in the midrange of the test.

The fact that the fatigue behavior of so many materials can be correlated by the da/dN vs ΔK plots suggests either that the deformation properties of the material have little influence on crack propagation or else that a single deformation process with a limited range of values is operative in all the materials for the range of conditions under which tests have been performed.

Linear elastic fracture mechanics threats materials as a perfect elastic continuum. Differences in material properties such as strength and ductility do not have a major influence on the analysis, even though it is clear from the examination of the fracture surfaces that some deformation is occurring prior to failure. Irwin has shown that this plasticity can be incorporated into the LEFM analysis by adjusting the crack length by the plastic zone size $r_p = C(\Delta K/\sigma_{ys})^2$.

The plastic zone size thus changes less than an order of magnitude over the range of ΔK values for the fatigue test. If the plastic zone size does not change appreciably and it the deformation mechanism controlling failure does not change, then perhaps the similarity of the fatigue crack propagation data in vacuum is not so surprising.

To examine the possible ways in which the deformation behavior of the material might influence the crack propagation behavior, another unifying principle is needed. The deformation mechanism map of Ashby [12] may provide such a tool if it can be adapted to failure behavior. Crack propagation in ductile materials is controlled by deformation in the localized region ahead of the crack tip, much as if the region were a miniature tensile specimen (strain-limited failure). Some insight into the possible processes that may occur can thus be gained by looking at analogous behavior in deformation of bulk samples. Ashby [12] has suggested a useful way of classifying deformation in normalized stress and temperature space (σ/μ and T/T_M) by mapping the regions in which different mechanisms control the deformation process. The deformation mechanism map for nickel, which has been extensively studied and which should be similar to maps for stainless steels, is shown in Fig. 10a. Most materials show the same general mechanism fields although the extent of the various fields may differ somewhat. Note that dislocation glide occurs above the yield strength at all temperatures. Also, a large elastic regime is present at all temperatures. In fact, the boundary of the elastic region is determined by the ability to detect plastic strain. At elevated temperatures (about 0.45 T_M), dislocation creep, Coble creep (diffusional flow by grain boundary transport), and Nabarro-Herring creep (diffusional flow by bulk diffusion) appear. There may be additional mechanisms, depending on whether grain boundary sliding is a separate mechanism or a form of Coble creep. Deformation mechanism maps show at a glance the possible mechanisms that may control deformation for a given set of test conditions.

A partial deformation mechanism map for AISI 304 Stainless Steel conditions, with isostrain-rate lines indicated, is shown in Fig. 10b [13]. It is similar to the map for nickel. The test temperatures used in the current tests, which correspond to homologous temperatures of 0.42 T_M and 0.52 T_M, that show plastic deformation might occur by Coble creep, dislocation creep, dislocation glide, or some combination of mechanisms, depending on the stress level (Fig. 10b). Stresses ahead of the crack may vary from somewhere in the elastic regime to something over the yield stress, depending on the loading conditions and the stress concentration ahead of the crack. This difficulty in defining the region that controls the deformation and the stress level in that region make it impossible to apply the deformation map formalism quantitatively to failure behavior. There is also the possibility that the mechanism controlling deformation does not influence the failure behavior. However, if deformation is by Coble creep rather than by dislocation motion, this should be evident in SEM observations of the fracture surface. Other distinctions may also be possible after more detailed study.

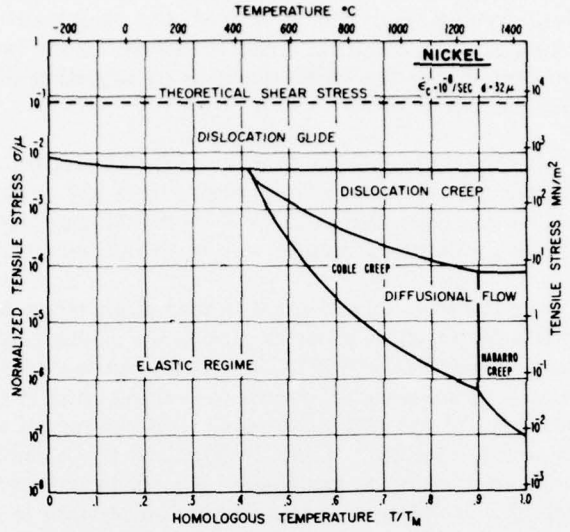

(a)

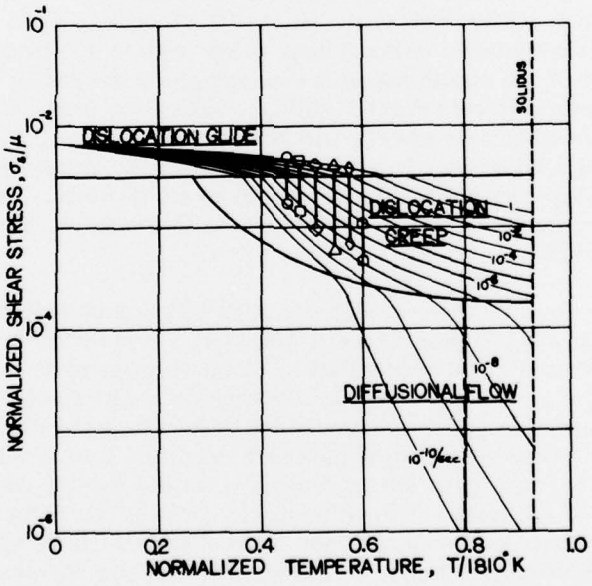

(b)

Fig. 10 — (a) Deformation mechanism map for nickel [12]: (b) deformation mechanism map for Type 304 stainless steel [13]

The discussion up to this point has established that fatigue crack propagation in vacuum for temperatures below 0.4 T_M follows fairly well-defined trends which depend on the K level and number of cycles. However, above 0.4 T_M, the possibility of time-dependent processes must be considered. Hold-time tests are often employed in an attempt to separate the cyclical component of crack growth from the time-dependent component. Hold-time tests are often analyzed by plotting da/dN vs ΔK and da/dt vs ΔK. If the hold time produces a deviation in da/dN vs ΔK from that in purely cyclic tests, then it is concluded that a time-dependent process is present. Likewise if da/dt vs ΔK curves for both hold time and static loading show the same behavior, then only a time-dependent process would be occurring. The first approach is useful for defining a threshold for time-dependent processes. There are serious difficulties with the second approach, however, because deformation relaxes the crack-tip stress intensity, and the assumptions upon which the definition of ΔK are based are no longer valid. Haigh [14], for one, has reviewed several sets of test data for this regime and shown the LEFM approach to be in valid. He suggests that there are two reasons for the surprisingly good correlation between da/dt and ΔK in such tests. The first is an implicit dependence of the ΔK factor on stress, and the second is the narrow range of K/σ values found for most test specimens; as a result the tests do not show large differences in stress relaxation during the test.

Landes and Begley [15] and Dowling and Begley [16] have examined possible approaches to a more general treatment of fatigue crack growth where gross plastic deformation occurs and the LEFM formulation is not valid. Such an approach directly acknowledges the inability to separate cyclic and creep deformation at elevated temperatures and provides the formalism for treating both together in the same test. However, J-integral tests are still in the development stage, and they are not as simple and direct as current fatigue test methods, so a practical approach is still to be developed.

Time dependence in fatigue tests may arise from either time-dependent deformation processes or time-dependent environmental attack. Spiedel [9] has reviewed the literature of these effects and has shown that fatigue tests conducted in air typically show an increase in crack growth rate by a factor of 2 or 3 over tests conducted in a vacuum at room temperature This increase in growth rate usually does not change the slope of the log da/dN vs log ΔK curves; it simply translates them to faster growth rates. Elevated temperature tests under conditions where oxidation is severe often show additional increases in growth rate, frequently accompanied by the onset of intergranular failure. The time dependence of environmental attack in air could arise from growth of an oxide film or from diffusion of oxygen into the crack tip region, both time-dependent processes.

In conclusion, a survey of the literature of FCP indicates that most FCP data in vacuum with loading below the elastic limit fall in a narrow band when plotted as a function of log (da/dN) vs log ($\Delta K/E$). Deviations occur when the temperature is increased to the range in which time-dependent deformation is detectable during the time period of the loading cycle and when the tests are conducted in air. A consideration of deformation mechanism maps suggests that such maps may be useful in correlating the deformation processes in the plastic zone ahead of the crack with SEM observations of the fracture surface.

DISCUSSION OF TEST RESULTS

Reproducibility and Validity of Test Results

The fatigue crack propagation data derived from the tests described in this report exhibit changes in slope and shifts in crack growth rate. Some of these features can be correlated with physical processes and some cannot. It is therefore useful to examine some of the factors that influence the reproducibility and validity of the data so as to have some perspective on the significance of changes in slope and of relative comparisions of different tests. Three aspects of the test results will be considered: (a) the reproducibility of fatigue crack propagation data, (b) the significance of changes in slope in da/dN vs ΔK curves, and (c) the proximity of the applied stress to the yield stress. A number of experimental factors can introduce uncertainty into the test data and thus produce scatter in the data from one test to another. Probably one major source of uncetainty is inability to measure the true crack length inside the specimen and to properly allow for curvature in the crack front. Curvature of the crack front can be influenced by specimen geometry, stress concentrations from side grooves, local stress concentrations from inclusions, premature failure at inclusions, and possibly by other factors. Curvature of the crack front can be seen in arrest markings where the crack has temporarily been stopped. Although admittedly such markings show the curvature for a condition of crack arrest rather than motion, they can be used to estimate the uncertainties that might arise in the da/dN va ΔK curves from curvature of the crack front. The largest deviation in crack length (difference between the length at the surface and the length at the specimen center) observed in these specimens was 1 mm in the aged specimens tested at 593°C (1100°F) with a 1-min hold time. This deviation would produce an uncertainty in ΔK of about ±10% and a corresponding uncertainty in the crack growth rate (da/dN) of about ±20%. Other sources of error are the accuracy of the load measurement and application, which will vary with experimental apparatus, and the resolution limit for measuring the crack length. This latter is sometimes complicated by cracks that are poorly defined because of branching or intermittent growth, especially in the high-ΔK regime of the tests.

James [17] has reviewed the influence of specimen design on the scatter band for fatigue crack propagation data in annealed Type 304 stainless steel tested in air at room temperature. Ten different specimen designs gave results reproducible within a factor at 3.8 between the lowest and hightest values of da/dN. Experience at NRL on a single design specimen tested at elevated temperature in air shows better reproducibility with a scatter band about half that reported by James, or a factor of 2. Relative uncertainty during a single test is, of course, much less.

Another feature of interest in the test results is the change in slope exhibited by many of the log da/dN vs log ΔK curves. These changes in slope are especially pronounced in tests of solution-annealed material at 593°C (1100°F) for 0- and 0.1-min hold times, where a decrease in slope occurs at about 44 MPa$\sqrt{\text{m}}$ (40 ksi$\sqrt{\text{in.}}$). Lesser changes of slope are observed at the high-ΔK end of the curve.

As noted in the previous discussion of unifying principles, there is no mechanism in the LEFM analysis that would lead to a decrease in slope. If any change were to occur as a result of approaching the fracture toughness limit or plastic instability, it would be an increase in slope. SEM examination of the fracture surface of the zero-hold-time specimen in the area

corresponding to the decrease in crack growth rate reveals no features markedly different from those in the low-ΔK end of the curve, although there is a change in the extent of intergranular failure at about 33 MPa$\sqrt{m}$ (30 ksi$\sqrt{in}$). Another possible cause for a decrease in slope at the high-ΔK end of the test is the relaxation of stress intensity due to creep and the resultant failure of the assumptions for valid ΔK measurements. This would tend to make the ΔK values calculated from the load higher than the true ΔK, if it still had any significance. Crack branching and intermittent cracking ahead of the main crack are occasionally noted in the high-ΔK portion of elevated temperature tests, and this too would invalidate the analysis beyond that point. The cause of the slope changes in the high-ΔK end of the tests has not been uniquely identified, but there appears to be a strong possibility that these effects originate in test conditions or procedures, and therefore no great significance should be ascribed to them until contrary evidence is found.

The final question of concern regards the stress range in the region ahead of the notch and the proximity of this stress to yield stress. The nominal stress σ_N ahead of the crack can be estimated from the flexural formula for beam bending. The nominal stress is given by

$$\sigma_N = \frac{6PL}{B(W\text{-}a)}$$

where L is the distance from the crack plane to the point of load application, W is the specimen width, a is the total crack length, B is the specimen thickness, and P is the applied load. At 427°C (800°F), the formula yields a nominal stress value of about 139 MPa (20 200 psi) at the beginning of the test, corresponding to a ΔK of about 22 MPa$\sqrt{m}$ (20 ksi$\sqrt{in.}$), and a nominal stress value of about 416 MPa (60 400 psi) toward the end of the test at a corresponding ΔK value of 66 MPa$\sqrt{m}$ (60 ksi$\sqrt{in.}$). Similarly, at 593°C (1100°F), the formula yield values of 108 and 351 MPa (15,700 and 59,900 psi) in the lower 22 MPa$\sqrt{m}$ (20 ksi$\sqrt{in.}$) and upper 66 MPa$\sqrt{m}$ (60 ksi$\sqrt{in.}$) ends of the test. These nominal stress values would exceed the 0.2% off set yield stress σ_{ys} for solution-annealed 316 steel, at 427°C (800°F), by 1.15 at the start of the test and increase to about 3.7 σ_{ys} at the end of the test [18]. At 593°C (1100°F) the ratio of σ_N/σ_{ys} goes from about 0.9 to 3, respectively. The stress concentration ahead of a notch in the triaxial stress state is approximately a factor of 3 higher than the uniaxial yield stress, so the initial portions of the tests are well within the elastic limit, but the end of the test may exceed the elastic limit.

Solution-Annealed Material Tested at 427°C (800°F)

The first question of concern in classifying the fatigue behavior in austenitic alloys is the influence of the air environment on the fatigue behavior. Although for all the specimens examined in this report the tests were conducted in air, some data on vacuum tests and tests in inert environments are available in the literature, and they provide a base line for comparison. The review of the data available on austenitic alloys by James [17] shows that, for tests conducted in vacuum or in an inert environment, the crack propagation rate increases only slightly when the temperature is increased from room temperature to 650°C (1200°F). In contrast to the data from vacuum tests, tests in air show an increase in crack growth rate with increasing temperature [17]. A comparision of data from vacuum tests on solution-annealed Type 316 at 538°C [17] with the NRL results on crack propagation in air at 427°C (800°F) shows

roughly a factor of 3 increase in crack propagation rate in the air tests. Smith et al. [19] have studied the effect of oxygen pressure on crack growth rate in 316 stainless steel using resonance fatigue specimens at 500°C (932°F) and 800°C (1482°F). Their study showed that increasing the oxygen pressure over the range 1.33×10^{-4} N/m^2 (10^{-6} torr) to 1.08×10^{-5} N/m^2 (810 torr) caused an increase in crack growth rate of 1 to 2 orders of magnitude compared to the vacuum tests. The crack growth rate appeared to increase with increasing oxygen pressure until monolayer coverage of newly exposed surface occurred during the cycle time of the test. Further increases in oxygen pressure did not produce an additional increase in crack growth rate. The crack path was observed to be transgranular for all oxygen pressures.

The SEM observations of the solution-annealed Type 316 tested at 427°C (800°F) in the present experiments showed a ductile failure mode propagating transgranularly. At higher magnifications, striations typical of those expected for a ductile material were observed. The striation spacing increased with crack length and correlated well with the calculated macroscopic crack growth rate (Figs. 3 and 4). Although SEM observations of the fracture surface were not reported for the vacuum tests cited in [17], it should be reasonable to assume the failure mechanism in that case was also a ductile tearing and that striation markings were also present. In air, 427°C (800°F) an oxide layer appears to form which accelerates the crack growth rate by a factor of 2 to 3 but produces no readily visible microstructural feature that would distinguish it from FCP in vacuum. Hold times up to 1 min do not accelerate the growth rate per cycle, nor is any evidence of a change in microstructure seen, thus indicating neither a time-dependent deformation process nor a time-dependent environmental attack in the time period from 0.1 to 1 min. It is also interesting to note that a careful examination of the surface along the entire crack length shows no indication of a change in deformation mode as the crack length increases (ΔK and σ_N increase). These observations indicate that the same failure process controlled during the entire test and that general yield was not exceeded in the triaxial stress state.

Solution-Annealed Material Tested at 593°C (1100°F)

An increase in test temperature from 427°C (800°F) to 593°C (1100°F) produced an order-of-magnitude increase in the crack growth rate in solution-annealed Type 316 tested in air at ΔK levels comparable to the 427°C (800°F) test. Imposition of 0.1-min and 1.0-min hold times progressively increased the crack growth rate. Above 44 MPa$\sqrt{\text{m}}$ (40 ksi$\sqrt{\text{in.}}$) the zero-hold-time curve showed a well-defined change in slope to much lower growth rates. SEM observations of the fracture surface of the zero-hold specimen at various points along the crack path showed patches where intergranular failure had occurred at crack lengths up to 1.65 cm (0.65 in.) which corresponds to a ΔK value of 33 MPa$\sqrt{\text{m}}$ (30 ksi$\sqrt{\text{in.}}$). Beyond this point the fracture path was entirely transgranular (Fig. 6). Imposition of a 1-min hold time increase the proportion of the surface characterized by intergranular failure (Fig. 7) so that at crack lengths below 33 MPa$\sqrt{\text{m}}$ (30 ksi$\sqrt{\text{in.}}$) the failure mode was 100% intergranular. Above 33 MPa$\sqrt{\text{m}}$ (30 ksi$\sqrt{\text{in.}}$) a large proportion of the surface was characterized by intergranular failure, but a few grains exhibited a transgranular crack path.

The increase in crack growth rate upon increasing the test temperature from 427°C (800°F) to 593°C (1100°F) and the further increase in crack growth rate upon application of a 1-min hold time are clearly associated with a change in failure mode from transgranular to intergranular. It is not clear from these tests alone whether the intergranular failure results from a

diffusional flow deformation process or from environmental attack, which causes grain boundary embrittlement. The question of the causitive mechanism would most clearly be resolved if vacuum tests on the same material were available. Although no information is available on microstructures, the literature results previously cited on austenitic stainless steels tested in vacuum [17] show only minor increases in crack growth rate for an increase in test temperature from 427°C (800°F) to 593°C (1100°F). This would tend to indicate that the increase in crack growth rate is due to environmental attack rather than diffusional flow creep processes.

A few qualitative calculations were made to evaluate the possibility of grain boundary embrittlement due to diffusion of oxygen into the material. One of the most significant of the SEM observations was the transition in failure mode from intergranular to transgranular. If this transition was caused by embrittlement due to oxygen diffusion, then the transition point should provide some measure of the diffusion rate required for embrittlement to occur.

The SEM micrographs of the solution-annealed specimen at 593°C (1100°F) with no hold time showed that after the crack had grown to about 1.625 cm (0.65 in.), the intergranular islands disappeared and thereafter the material failed transgranularly. The fatigue data showed that at a crack length of 1.625 cm (0.65 in.) the crack growth rate da/dN is 2×10^{-4} cm/cycle. For the cycle time of 6 s the effective crack growth rate is approximately 3×10^{-5}cm/s. At the temperature of interest, grain boundary diffusion is more rapid then bulk diffusion, so a comparison of the above rate with a surface diffusion model should provide some indication of the applicability of the concept. An estimate of the surface diffusivity was made for a random walk diffusion model where the root-mean-square diffusion distance $\overline{R}$ is given by $(4\ Dt)^{1/2}$. If $\overline{R}$ is taken as 2×10^{-4}cm and t is 6 s, then the diffusivity is 1.7×10^{-9}cm^2/s. Data on the grain boundary diffusivity of oxygen in stainless steel were not available, but a composite equation for grain boundary diffusivity in fcc metals has been developed by Gjostein [20] and was used for comparison. This equation gives a grain boundary diffusion coefficient of about 4×10^{-9} cm^2/s for 593°C. Considering the approximations involved, this is excellent agreement between model and experiment.

An examination of some of the other conditions further confirms consistency with the model. For example, if one uses Gjostein's value for diffusivity in the random walk equation, an approximate penetration distance per cycle can be calculated. At 593°C (1100°F) for the 1-min hold time, it is found that the penetration distance per cycle is $\approx 1 \times 10^{-3}$cm, which exceeds the crack growth rate per cycle for all except the very highest values of ΔK. This is consistent with the observation that intergranular failure is observed along the entire crack path in this specimen. At 427°C (800°F), Gjostein's value for D_{GB} is 5×10^{-11}cm^2/s. This yields a penetration distance of $\approx 1 \times 10^{-5}$cm for the 1-min hold-time test, which is less than the crack growth rate per cycle for all except the very lowest ΔK values. Again this is consistent with the absence of intergranular failure in the 427°C (800°F) tests.

An analysis of fatigue crack propagation behavior of the solution-annealed Type 316 stainless steel tested in air at 593°C (1100°F) suggests that the growth rate is strongly influenced by embrittlement of the grain boundaries as a result of diffusion of oxygen along grain boundaries ahead of the growing crack. This conclusion is reached because (a) the increase in crack growth rate with temperature is much greater in air than in vacuum, and (b) an intergranular failure mode occurs under conditions where the penetration distance for oxygen diffusion along grain boundaries exceeds the crack growth rate per cycle.

Aged Material Tested at 593°C (1100°F)

The aging of Type 316 stainless steel at 593°C (1100°F) for 5000 h resulted in a decrease in crack growth rate as compared to the solution-annealed material tested at 593°C (1100°F) described above. In addition, hold times up to 1.0 min imposed on the loading cycle had no effect on crack growth rate. SEM examination of the specimens showed the crack path to be transgranular in all tests, although it showed a ductile rupture type of failure. Since the opportunity for environmental attack is the same for both material conditions, it can be concluded that the aging treatment has strengthened the grain boundaries so that they are no longer the point of failure initiation even when embrittled by penetration of the oxygen. This is consistent with the precipitation of $M_{23}C_6$ carbides along grain boundaries, which would be expected to occur in austenitic stainless steels given this heat treatment [21]. The precipitate structure is readily visible in the SEM micrographs. The crack growth rate was approximately the same as that observed in the 427°C (800°F) test of solution-annealed material at ΔK values below 44 MPa$\sqrt{m}$ (40 ksi$\sqrt{in}$). This implies that the controlling deformation process must be similar in nature to that in the 427°C (800°F) test of the solution-annealed material. This conclusion is reached in spite of the fact that the predominant features observed in the SEM examination of the surface were microvoids which had nucleated at precipitates and then ruptured by tearing the ligaments between the voids. Fatigue striations can be seen at the high-ΔK end of the specimen, and they can also be seen at the low-ΔK end of the specimen when the surface is still covered with a light film of oxide. The fatigue striations are not easily seen after the surface is cleaned, apparently because the microvoids are of the same size as the striation markings. The irregularity of the surface around the microvoid tends to obscure the striations except when they are covered with a thin layer of oxide that reveals the topographic relief. The formation and coalescence of microvoids seem to influence only the final failure process and indicate a matrix that has good ducility but has some reduction in overall specimen ductility due to early initiation of voids at the precipitates (Fig. 8 and 9). The imposition of hold time on the loading cycle does not produce any significant change in the appearance of the fracture surface. This is consistent with the fatigue data which showed no hold-time effect.

COMPARISON OF MODEL WITH PREVIOUS INTERPRETATIONS

The model of FCP developed in the current study with the additional information provided by SEM characterization of the fracture surfaces is as follows:

- Fatigue crack propagation data for annealed Type 316 stainless steel can be described in terms of the empirical relationship, $da/dN = C(\Delta K/E)^n$. Data for tests conducted in vacuum at temperatures up to 600°C can be described by the same curve and should show no hold-time effects. The introduction of air causes an immediate increase in crack growth rate by a factor of 3 at all temperatures from room temperature up to at least 430°C. In this temperature range the crack path is transgranular and the air environment produces no change in surface appearance. In addition, no hold-time effects are observed in the above temperature range for times up to 1 min. An increase in temperature to 600°C causes embrittlement of the grain boundaries as a result of diffusion of oxygen along the grain boundaries, a change to an intergranular mode of failure, and an accompanying increase in crack growth rate.

The degree of intergranular failure is controlled by the distance that the oxygen can diffuse ahead of the crack tip during a cycle, so the crack growth rate, hold time, and temperature all influence the extent of embrittlement. Aging the material produces precipitation both at the grain boundaries and in the matrix. Strengthening of the grain boundaries is such that intergranular failure is no longer favored at 600°C and no hold-time effects are observed.

- An upper limit to the ΔK range is imposed by K_{Ic}, and the slope of the curve should increase rapidly as this limit is approached. No inflection points in the curves would be predicted from the analysis of LEFM, and no change in microstructural features was observed that could be correlated with the inflection points observed in some of the curves.

The principal questions open to discussion in these results are as follows

(1) The existence of a general behavior trend that describes all the results

(2) The cause of the increased crack growth rate in the solution-annealed material when the test temperature is raised from 427° (800°F) to 593°C (1100°F)

(3) The origin of the hold time effects in the solution-annealed material at 593°C (1100°F)

(4) The effect of aging on the fatigue crack propagation behavior at 593°C (1100°F)

(5) The significance of the sharp changes in slope exhibited in a number of the fatigue curves.

Discussions and interpretations of the test results in the previous publications [1-3] are summarized and discussed for each of these questions. With regard to question 1, both Shahinian et al. [1] and Michel et al. [2,3] plotted the experimental data in the form of the log (da/dN) vs log ΔK curves to show generalized behavior trends. No clear distinction was made as to why air tests would show deviations from this behavior. Shahinian [11] had also noted that the temperature dependence of the crack growth could be explained by the temperature dependence of E for tests conducted in vacuum. Michel et al. [2] applied the oxygen adsorption model [19] to show that the surface of the crack would be covered by an oxygen monolayer at 427°C (800°F) and that this could produce an increase in crack growth rate over that expected in a vacuum test.

In questions 2 and 3, which are related, there is a difference of interpretation between the present model and that previously proposed in Refs. 1-3. Shahinian et al. [1] ascribe the accelerated crack growth rate at 593°C (1100°F) in air and the effects of hold time to the operation of creep processes. Michel et al. [2] made use of the oxygen adsorption model to show that the surface was saturated well below 427°C (800°F) and concluded that the air environment should produce no further change in the environmental frequency effect at higher temperatures. SEM evidence shows that there is a change in failure mode from transgraunlar to intergranular that accompanies these changes in test conditions, and we conclude that this change in mode is responsible for the increase in crack growth rate. Creep processes do occur in austenitic stainless steels at 593°C (1100°F), as can be seen from the Ashby deformation mechanism maps [12]. However, literature references [17] on crack propagation

tests on Type 316 stainless steel in vacuum show no increase in crack growth rate comparable to that observed in the air tests in going from 427°C (800°F) to 593°C (1100°F). The ultimate test for this question would be a vacuum test of the same heat of material as was used in the previous experiments [1-3], but the current evidence appears to support environmental attack of the grain boundaries.

Question 4, concerning the effect of aging on the crack growth rate at 593°C (1100°F), also is interpreted differently in previous publications. Michel and Smith [3] suggest that the crack growth in the aged material decreases from that in the solution-annealed material, possibly because of crack blunting by the precipitates in the matrix. The present authors suggest that the effect of aging is to strengthen the grain boundaries so as to suppress intergranular failure and that the transgranular crack growth rate observed in this specimen is in fact about what would be predicted if a correction for the temperature dependence of E were applied to the 427°C (800°F) data. It is further submitted that merely strengthening the matrix would increase rather than decrease the degree of intergranular failure observed in the solution-annealed material tested at 593°C (1100°F).

For question 5, concerning the changes in slope of the log (da/dN) vs log ΔK curves, the previous papers offer no interpretations, although Shanhinian comments in a paper on 304 stainless steel and cold-worked 316 [22] that crack branching or nucleation of cracks ahead of the main crack was sometimes observed near the end of the tests.

CONCLUSIONS

SEM examination of the fracture surfaces of fatigue specimens of Type 316 stainless steel previously tested at elevated temperatures in air [1-3] has provided some useful insight into the crack propagation behavior of this material. The specimens examined were in three basic combinations of material condition and test temperature — (a) solution-annealed material tested at 427°C (800°F), (b) solution-annealed material tested at 593°C (1100°F), and (c) material aged at 593°C (1100°F) for 5000 h and tested at 593°C (1100°F). Hold-time tests of 0.1 and 1 min were also conducted for each combination. Significant observations are as follows:

1. The solution-annealed material tested at 427°C 800°F exhibits fatigue striations indicative of ductile failure processes. Although test data indicated an acceleration in crack growth rate relative to vacuum tests cited in the literature, there was no obvious indication of a change in failure mechanism on the fracture surface.

2. The solution-annealed material tested at 593°C (1100°F) shows patches of intergranular failure in the low-ΔK range of the test. The percentage of intergranular failure increased with hold time and extended over the entire range of ΔK in the test for 1-min hold-time. An analysis of possible failure processes points toward environmental attack by diffusion of oxygen along grain boundaries as the responsible mechanism for the change to intergranular failure mode and the attendent increase in crack growth rate relative to the 427°C (800°F) test.

3. The aged material tested at 593°C (1100°F) exhibited a ductile rupture type of failure with microvoids nucleating on the precipitates which formed during aging. No

intergranular failure was observed and it was concluded that the aging treatment effectively strengthened the grain boundaries, preventing intergranular failure and to reducing the crack growth rate relative to the growth rate of solution-annealed material tested at 593°C (1100°F).

4. A consideration of possible causes for the inflection points in the log da/dN vs log ΔK curves did not uncover any mechanisms which might be responsible. Either crack branching or deformation, which would invalidate the fracture mechanics approach, seem to be the most probable causes for the inflection points, but this remains to be established conclusively.

ACKNOWLEDGMENTS

This work was supported by the Division of Reactor Research and Development of the Energy Research and Development Administration.

The authors wish to express their appreciation to Dr. J. A. Sprague and D. A. Meyn for assistance with the SEM observations and to Dr. D. J. Michel, Dr. P. Shahinian, and H. H. Smith for providing the samples from their tests and for helpful discussions on the manuscript.

REFERENCES

1. P. Shahinian, H. H. Smith, and H. E. Watson, "Fatigue Crack Growth Characteristics of Several Austenitic Stainless Steels at High Temperature," ASTM STP 520, ASTM pp. 387-397 (1973).

2. D. J. Michel, H. H. Smith, and H. E. Watson, "Effect of Hold-Time on Elevated Temperature Fatigue Crack Propagation in Fast Neutron Irradiated and Unirradiated Type 316 Stainless Steel," in *Structural Materials for Service at Elevated Temperature in Nuclear Power Generation*, A. O. Schaefer, ed., MPC-1, ASME 1975, pp. 167-190.

3. D. J. Michel and H. H. Smith, "Effect of Hold Time on Elevated Temperature Fatigue Crack Propagation in Types 304 and 316 Stainless Steel," in *Symposium on Creep-Fatigue Interactions*, R. M. Curran, Ed. MCP-3, ASME, 1976, pp. 391-415.

4. "SEM/TEM Fractography Handbook," Battelle Columbus Laboratories, Metals and Ceramics Information Center, MCIC-HB-06, Dec. 1975.

5. C. R. Brooks and C. D. Lundin, "Rust Removal From Steel Fractures-Effect on Fractographic Evaluation," Microstructural Science, vol. 3, Part A, edited by P. M. French, R. J. Gray and J. L. McCall, American Elsevier New York, 21-33 (1975).

6. S. M. McCoy, "Replica Techniques for Transmission Electron Microscopy," NRL memorandum Report 3220, Feb. 1976.

7. B. Gross, J. E. Srawley, "Stress-Intensity Factors for Single-Edge-Notch Specimens in Bending or Combined Bending and Tension by Boundry Collocation of Stress Function," NASA-TN-D2603, National Aeronautics and Space Admin., Washington, D. C., Jan. 1965.

8. C. Laird, ASTM Conf. on Fatigue Crack Propagation, Atlantic City, 131-168 (1966).

9. M. O. Speide, "Fatigue Crack Growth at High Temperature," High Temperature Materials in Gas Turbines, Elsevier, Amsterdam, 207-251 (1974).

10. P. C. Paris and F. Erdogan, J. Basic Eng. (Trans. MSME Series D) 855:528 (1963).

11. P. Shahinian, H. E. Watson, and H. H. Smith, *Journal of Materials*, 7:4, 527:535, Dec. 1972

12. M. F. Ashby, "A First Report on Deformation-Mechanism Maps," Acta Metallurgica, 20, 887-897, July 1972

13. R. K. Ravindra Bhargava, J. Moteff and R. W. Swindeman, "The Dislocation Substructure, Carbides and the Deformation Mechanism Map for AISI 304 Stainless Steel," Metallurgical Transactions A, 7A, 879-887, June 1976

14. J. R. Haigh, "The Mechanisms of Macroscopic High Temperature Crack Growth, Part II: Review and Re-analysis of Previous Work," Materials Science and Engineering, 20 225-235 (1975)

15. J. D. Landes and J. A. Begley, "A Fracture Mechanics Approach to Creep Crack Growth," in *Mechanics of Crack Growth*, ASTM STP 590, 128-148 (1976)

16. N. E. Dowling and J. A. Begley, "Fatigue Crack Growth During Gross Plosticety and the J-Integrel," in *Mechanics of Crack Growth*, ASTM STP 590, 82-103 (1976).

17. L. A. James, "Fatigue-Crack Propagation in Austenitic Stainless Steels," Atomic Energy Review 141, 37-86 (1976) published by IAEA, Vienna, Austria.

18. *Nuclear Systems Material Handbook*, vol. I, Design Data, Book 1, TID-26666, Property Code 2102, Hanford Engineering Development Laboratory, Richland, Wash., p. 10.

19. H. H. Smith, P. Shahinian, and M. R. Schter, "Fatigue Crack Growth Rates in Types 316 Stainless Steel at Elevated Temperatures as a Function of Oxygen Pressure," Transactions of the Metallurgical Society of AIME, 245, 947-953 (1969)

20. N. A. Gjostein, "Short Circuit Diffusion," *Diffusion*, Am. Soc. for Metals, 241-274 (1972).

21. B. Weiss and R. Stickler, "Phase Instabilities During High Temperature Exposure of 316 Austenitic Stainless Steel," Metallurgical Trans. 3, 851-866, Apr. 1972

22. P. Shahinian, "Creep-Fatigue Crack Propagation in Austenitic Stainless Steel," *Journal of Pressure Vessel Technology* Trans. ASME, 98, 166-172 (1976).